AD_____

Award Number: DAMD17-02-1-0725

TITLE: Structure-Based Design of Cdk4/6-Specific Inhibitors

PRINCIPAL INVESTIGATOR: Ronen Marmorstein, Ph.D.

CONTRACTING ORGANIZATION: The Wistar Institute
Philadelphia, Pennsylvania 19104

REPORT DATE: October 2006

TYPE OF REPORT: Final

PREPARED FOR: U.S. Army Medical Research and Materiel Command
Fort Detrick, Maryland 21702-5012

REPORT DOCUMENTATION PAGE

Form Approved
OMB No. 0704-0188

1. REPORT DATE *(DD-MM-YYYY)*	**2. REPORT TYPE**	**3. DATES COVERED** *(From - To)*
01-10-2006	Final	30 Sep 2002 – 29 Sep 2006

4. TITLE AND SUBTITLE

Structure-Based Design of Cdk4/6-Specific Inhibitors

5a. CONTRACT NUMBER

5b. GRANT NUMBER
DAMD17-02-1-0725

5c. PROGRAM ELEMENT NUMBER

6. AUTHOR(S)

Ronen Marmorstein, Ph.D.

E-Mail: marmor@wistar.org

5d. PROJECT NUMBER

5e. TASK NUMBER

5f. WORK UNIT NUMBER

7. PERFORMING ORGANIZATION NAME(S) AND ADDRESS(ES)

The Wistar Institute
Philadelphia, Pennsylvania 19104

8. PERFORMING ORGANIZATION REPORT NUMBER

9. SPONSORING / MONITORING AGENCY NAME(S) AND ADDRESS(ES)
U.S. Army Medical Research and Materiel Command
Fort Detrick, Maryland 21702-5012

10. SPONSOR/MONITOR'S ACRONYM(S)

11. SPONSOR/MONITOR'S REPORT NUMBER(S)

12. DISTRIBUTION / AVAILABILITY STATEMENT
Approved for Public Release; Distribution Unlimited

13. SUPPLEMENTARY NOTES

14. ABSTRACT

The CDK4/6 kinase has elevated activity in spontaneous breast cancer, making it an excellent candidate for targeted inhibition for the treatment of breast cancer. We proposed to prepare a CDK4/6-specific kinase inhibitor that is based on the naturally occurring CDK4/6 specific inhibitory proteins of the INK4 family. Since the INK4 proteins are notoriously unstable, we have been working towards the preparation and structural characterization of INK4 proteins with improved thermostability that could be used as a scaffold to prepare peptide sub-fragments that may serve as a scaffold to prepare "small molecule" CDK4/6-specific inhibitors. During the funding period, we successfully prepared p18INK4c proteins with increased thermostability and have characterized the structure of a subset of the more thermostable p18INK4c proteins. This structure-function analysis revealed the chemical basis for the increased stability properties of the more thermostable p18INK4c proteins. Significantly, a thermostable F71N mutant protein also showed enhanced CDK6 interaction and cell cycle inhibitory activity in vivo, as measured using co-immunoprecipitation and transient transfection assays, respectively. Together, our studies show that a structure-based approach to increase the thermodynamic stability of INK4 proteins can be exploited to prepare more biologically active molecules with potential applications for the development of molecules to treat INK4-mediated cancers.

15. SUBJECT TERMS
breast cancer

16. SECURITY CLASSIFICATION OF:			**17. LIMITATION OF ABSTRACT**	**18. NUMBER OF PAGES**	**19a. NAME OF RESPONSIBLE PERSON**
a. REPORT	**b. ABSTRACT**	**c. THIS PAGE**			USAMRMC
U	U	U	UU	16	**19b. TELEPHONE NUMBER** *(include area code)*

Table of Contents

(5) INTRODUCTION

Distinct cancer types have been correlated with several proteins that are involved in the G1 to S transition of the mammalian cell cycle (Funk, 1999; Molinari, 2000). In particular, the inability to inhibit the activity of the paralogs, cyclin-dependent kinases 4 and 6 (CDK4/6) are implicated in more than 80% of human neoplasias (Ortega et al., 2002). For example, the gene encoding the CDK4/6 inhibitory protein, $p16^{INK4}$, is deleted or mutated in the majority of leukemias, bladder cancers and familial melanomas (Roussel, 1999). The CDK4/6 stimulatory subunit, cyclin D1, is commonly found to be overexpressed or gene amplified in spontaneous breast cancers (Donnellan and Chetty, 1998; Khoo et al., 2002), and overexpression of cyclin D1 in mice leads to death due to breast cancer (Wang et al., 1994). Finally, CDK4 itself is overexpressed or gene amplified in about one third of breast cancers (Ortega et al., 2002). Together, these observations indicate that deregulation of the G1 to S transition of the mammalian cell cycle is tightly linked to the onset of several different cancer types, and that the CDK4/6 protein, in particular, is an excellent candidate for targeted inhibition for the treatment of breast cancer.

The vast majority of currently available CDK4/6 inhibitors have structural similarity to the common kinase cofactor ATP and, as a result of this, a major obstacle in developing these inhibitors into clinically useful drugs is overcoming harmful side effects due to a lack of CDK4/6 specificity (Toogood, 2001). Here, we propose to prepare a CDK4/6-specific kinase inhibitor that is based on the naturally occurring CDK4/6 specific inhibitory proteins of the INK4 family (Carnero and Hannon, 1998). Towards this goal, we have previously determined the structure of the INK4 protein $p18^{INK4c}$ revealing 5 contiguous ankyrin-like repeats (Venkataramani et al., 1998). Another structure of CDK6 in complex with $p18^{INK4c}$ that was reported by Jeffrey et al. (Jeffrey et al., 2000) reveals that repeats 2 and 3 mediate most of the inhibitory interactions with CDK6. Based on these results, we hypothesize that a modified and truncated $p18^{INK4c}$ protein (INK4-mod_{2-3}) could be prepared harboring only ankyrin-like repeats 2 and 3 in addition to amino acid substitutions that enhance the proteins CDK4/6 inhibitory activity. Modifications in $p18^{INK4c}$ would include amino acid substitutions that increase the stability of the inhibitory domain in order to raise the likelihood of autonomous folding, and to increase the affinity of $p18^{INK4c}$ for CDK4/6. INK4-mod_{2-3} would then serve as a potent CDK4/6-specific peptide inhibitor itself as well as an excellent scaffold for the design of even smaller peptide or small molecule non-peptidic mimics that might have clinical application for the specific inhibition of CDK4/6 for the treatment of breast cancer.

The Specific Aims of the proposal were to (1) Prepare and characterize site-directed mutants of $p18^{INK4c}$ with increased protein thermostability, association with CDK4/6, and cell-cycle inhibitory activity *in vivo*, (2) Prepare an autonomous ankyrin-like region 2-3 peptide derived from the optimally modified $p18^{INK4c}$ (INK4-mod_{2-3}) protein prepared in aim 1, (3) Determine the X-ray crystal structure of INK4-mod_{2-3} in complex with CDK6, and (4) Use the structural information from the CDK6/ INK4-mod_{2-3} complex to initiate the structure-based design of peptide or small molecule non-peptidic mimics of INK4-mod_{2-3}.

(6) BODY

During the first year of the funding period we completed most of Aim1 (Tasks 1-3) to prepare and characterize site directed mutants of $p18^{INK4c}$ with increased protein thermostability, association with CDK4/6 and cell-cycle inhibitory activity. Specifically, we used a combination of structure-based mutagenesis, structural studies, and *in vitro* and *in vivo* studies to identify three $p18^{INK4c}$ mutant proteins with increased protein thermostability and CDK4/6 inhibitor activity, F71N, F82Q and F92N. Of these three $p18^{INK4c}$ mutant proteins the F71N mutant showed the most significant enhancement in protein stability and CDK4/6 inhibitory activity. A manuscript describing these studies was published in the *Journal of Biological Chemistry* and is included in the Appendix of this report (Venkataramani et al., 2002).

An assumption of the studies with $p18^{INK4c}$ was that the mutations that stabilize this member of the INK4 proteins would also stabilize the $p16^{INK4a}$ protein, thereby allowing us to use $p18^{INK4c}$ as a suitable model system for designing small $p16^{INK4a}$ mimics for CDK4/6 inhibition. We spent the second year of the funding period testing this assumption by preparing $p16^{INK4a}$ mutations that correspond to the F71N, F82Q and F92N mutations prepared for $p18^{INK4c}$. Therefore, we prepared the $p16^{INK4a}$ mutant proteins T79Q, T79N, F90N and A100N. Each of these mutant proteins were prepared by site-directed mutagenesis, and the proteins overexpressed in bacteria as inclusion bodies. The proteins were then solubilized by suspending them in 6M urea and refolded them by dialysis against a buffer in the absence of urea. Each of the soluble and refolded proteins was chromatographed on gel filtration using a Superdex-75 column. Surprisingly, we found that while the majority of the native $p16^{INK4a}$ protein chromatographs as a monomeric protein, each of the mutants show a large percentage of protein in the aggregated form (in the void volume of the column), suggesting that each of the $p16^{INK4a}$ mutants that we prepared are less stable than the native protein. Crystallization trails with each of these $p16^{INK4a}$ mutant proteins were also unsuccessful. Based on these studies, we concluded that $p18^{INK4c}$ may not serve as a suitable model for designing more thermostable $p16^{INK4a}$ proteins. In light of this, we have now modified our Aims to directly study site-directed mutations and protein truncations in $p16^{INK4a}$, rather than $p18^{INK4c}$.

While we were designing stabilizing mutations in $p16^{INK4a}$, we noted a manuscript published by Peng and colleagues in which the authors used several complementary techniques to identify three stabilizing mutations in $p16^{INK4a}$ (Cammett et al., 2003). These mutations are W15D, L37S and L121R. Interestingly a combination of these stabilizing mutations (called HTM for hyperstable triple mutant) has an additive thermostability with the HTM mutant being 1.4 kcal/mol more stable than the wild-type protein. In addition, the HTM $p16^{INK4a}$ mutant was able to rescue the oncogeneic R24P, P81L and V126D $p16^{INK4a}$ mutants for CDK4 binding. We decided to take advantage of these seminal findings by preparing the HTM $p16^{INK4a}$ mutant protein for our studies. We therefore spent the third year of the funding period working on the HTM $p16^{INK4a}$ mutant with the following goals in mind (1) Prepare a recombinant form of the HTM $p16^{INK4a}$ mutant, and (2) purify and crystallize the HTM-$p16^{INK4a}$ protein and determine its three dimensional structure. We hypothesized that the HTM $p16^{INK4a}$ structure would serve as a structural scaffold for Aims 2 and 3 of the initial proposal.

During the third year of the funding period we have successfully employed site directed mutagenesis to prepare the recombinant HTM-p16^{INK4a} protein and have purified the protein to homogeneity using a combination of ion-exchange and gel filtration chromatography (Figures 1a and 1b). We have carried our crystallization trails with this protein with several different factorial screens, initially at two different temperatures, 18 °C and 4 °C. The crystallization factorial screens (Cudney et al., 1994; Jancarik and Kim, 1991; Scott et al., 1995) that we employed were from Hampton Research, Molecular Dimensions, Jena Bioscience and DeCode Genetics. In addition, we employed grid screens, in which various precipitants were titrated as a function of pH, supplied by Hampton Research. Using this strategy, we have recently obtained several preliminary crystal forms (Figure 1c). A common factor with the conditions that produce crystals is that they are formed at 4 °C and with the precipitating agent PEG 3.5K. Over the coming year we will use crystallization refinement strategies to improve the quality of these crystals so that they can be analyzed using X-ray crystallography. We then plan to determine the X-ray crystal structure of HTM-p16^{INK4a} and to use it as a scaffold for accomplishing Aims 2 and 3 of the initial proposal.

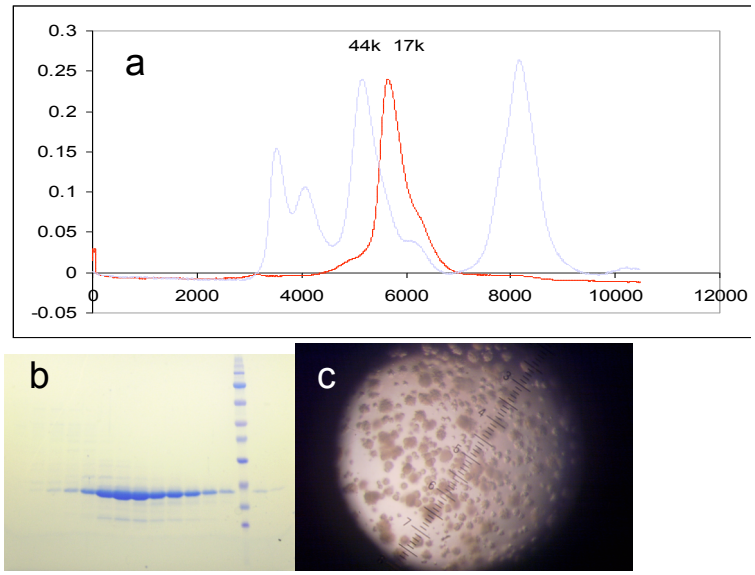

Figure 1. Preparation of preliminary crystals of HTM-p18^{INK4a}. (a) Gel filtration chromatography of the protein (red) overlaid with molecular weights standards (blue). (b) SDS-PAGE showing the elution of homogeneous HTM-p18^{INK4a} across the peak. (c) Preliminary crystals of HTM-p18^{INK4a}.

(7) KEY RESEARCH ACCOMPLISHMENTS

Year 1

- Prepared recombinant p18^{INK4c} mutant proteins with increased stability and CDK4/6 inhibitory activity.
- Carried out a detailed functional characterization of these p18^{INK4c} mutant proteins to identify the more stable F71N, F82Q and F92N mutants.
- Determined the X-ray crystal structure of three of the most thermostable p18^{INK4c} mutants, F71N, F82Q and F92N.
- Identified the F71N p18^{INK4c} mutant as a promising lead stability mutant for further characterization.

Year 2

- Prepared recombinant p16^{INK4a} mutant proteins (T79Q, T79N, F90N and A100N) that were predicted to have increased thermal stability.

- Characterized the gel filtration behavior of the $p16^{INK4a}$ mutants described above leading to the conclusion that the INK4 protein $p18^{INK4c}$ does not serve as a good model for designing more thermostable $p16^{INK4a}$ proteins.

Year 3

- Prepared recombinant HTM-$p16^{INK4a}$ mutant protein and purified this protein to homogeneity for crystallization efforts.
- Prepared preliminary crystals of HTM-$p16^{INK4a}$.

(8) REPORTABLE OUTCOMES

Venkataramani, R.N., MacLachlan, T.K, Chai, X., El-Deiry, W.S. and Marmorstein, R. "Structure-Based Design of More Stable $p18^{INK4c}$ Proteins with Increased CDK Inhibitory Activity." (2002), *J. Biol. Chem.*, 277, 48827-48833.

(9) CONCLUSIONS

During the first year of the funding period we have successfully completed tasks 1-3 of the proposal. Specifically, we have prepared $p18^{INK4c}$ mutant proteins that harbor increased protein stability and CDK4/6 inhibitory activity. During the second year of the funding period we addressed whether the INK4 protein, $p18^{INK4c}$, serves as a good model system for understanding the structure and stability of $p16^{INK4a}$ and discovered that it does not. During the third year of the funding period we prepared a thermostable $p16^{INK4a}$ variant called HTM-$p16^{INK4a}$ and have obtained preliminary crystals of this protein. Over the coming year we will use crystallization refinement strategies to improve the quality of these crystals and the resulting refined crystals for X-ray structure determination of HTM-$p16^{INK4a}$. We will then use the HTM-$p16^{INK4a}$ structure as a scaffold to accomplish Aims 2 and 3 of the initial proposal.

Since the hyperactivity of the CDK4/6 kinase is associated with a large number of cancers including a significant number of breast cancers, CDK4/6 is a highly relevant target for the development of inhibitory compounds that may provide effective therapeutics for the treatment of breast cancer. Unfortunately, the vast majority of currently available CDK4/6 inhibitors have structural similarity to the common kinase cofactor ATP and, as a result of this; a major obstacle in developing these inhibitors into clinically useful drugs is overcoming harmful side effects due to a lack of CDK4/6 specificity. Our use of the INK4 family as a scaffold will result in the preparation of peptide inhibitors of CDK4/6 with enhanced specificity. The preparation of these initial peptides will than lead to a set of lead peptides or non-peptidic compounds that can be further developed using combinatorial chemistry approaches (Beeley and Berger, 2000; Kirkpatrick et al., 1999; Leach et al., 2000; Roe et al., 1998). High affinity compounds developed through this approach can then be tested in cell culture systems and ultimately through clinical trials to treat CDK4/6-mediated breast cancers.

(10) REFERENCES

Beeley, N., and Berger, A. (2000). A revolution in drug discovery. Combinatorial chemistry still needs logic to drive science forward. BMJ *321*, 581-582.

Cammett, T. J., Luo, L., and Peng, Z. Y. (2003). Design and characterization of a hyperstable p16INK4a that restores Cdk4 binding activity when combined with oncogenic mutations. J Mol Biol *327*, 285-297.

Carnero, A., and Hannon, G. J. (1998). The INK4 family of CDK inhibitors. Curr Top Microbiol Immunol *227*, 43-55.

Cudney, R., Patel, S., Weisgraber, K., Newhouse, Y., and McPherson, A. (1994). Screening and optimization strategies for macromolecular crystal growth. Acta Cryst *D50*, 414-423.

Donnellan, R., and Chetty, R. (1998). Cyclin D1 and human neoplasia. Mol Pathol *51*, 1-7.

Funk, J. O. (1999). Cancer cell cycle control. Anticancer Res *19*, 4772-4780.
Jancarik, J., and Kim, S.-H. (1991). Sparse matrix sampling: a screening method for crystallization of proteins. J Appl Crystalog *24*, 409-411.

Jeffrey, P. D., Tong, L., and Pavletich, N. P. (2000). Structural basis of inhibition of CDK-cyclin complexes by INK4 inhibitors. Genes Dev *14*, 3115-3125.

Khoo, M. L., Ezzat, S., Freeman, J. L., and Asa, S. L. (2002). Cyclin D1 protein expression predicts metastatic behavior in thyroid papillary microcarcinomas but is not associated with gene amplification. Journal of Clinical Endocrinology & Metabolism *87*, 1810-1813.

Kirkpatrick, D. L., Watson, S., and Ulhaq, S. (1999). Structure-based drug design: Combinatorial chemistry and molecular modeling. Comb Chem High Throughput Screen *2*, 211-221.

Leach, A. R., Bryce, R. A., and Robinson, A. J. (2000). Synergy between combinatorial chemistry and de novo design. Journal of Molecular Graphics & Modelling *18*, 358-367.

Molinari, M. (2000). Cell cycle checkpoints and their inactivation in human cancer. Cell Prolif *33*, 261-274.

Ortega, S., Malumbres, M., and Barbacid, M. (2002). Cyclin D-dependent kinases, INK4 inhibitors and cancer. Biochimica et Biophysica Acta *1602*, 73-87.

Roe, D. C., Kick, E. K., Skillman, A. G., Liu, G., and Ellman, J. A. (1998). Combining structure-based drug design with combinatorial chemistry. Abstr Pap Am Chem Soc *216*, 011-COMP.

Roussel, M. F. (1999). The INK4 family of cell cycle inhibitors in cancer. Oncogene *18*, 5311-5317.

Scott, W. G., Finch, J. T., Grenfell, R., Smith, J. F. T., Gait, M. J., and Klug, A. (1995). Rapid crystallization of chemically synthesized hammerhead RNAs using a double screening procedure. J Mol Biol *250*, 327-332.

Toogood, P. L. (2001). Cyclin-dependent kinase inhibitors for treating cancer. Medicinal Research Reviews *21*, 487-498.

Venkataramani, R., Swaminathan, K., and Marmorstein, R. (1998). Crystal structure of the CDK4/6 inhibitory protein $p18^{INK4c}$ provides insights into ankyrin-like repeat structure and function and tumor-derived $p16^{INK4}$ mutations. Nature Struc Biol *5*, 74-81.

Venkataramani, R. N., MacLachlan, T. K., Chai, X., El-Deiry, W. S., and Marmorstein, R. (2002). Structure-based design of p18INK4c proteins with increased thermodynamic stability and cell cycle inhibitory activity. J Biol Chem *277*, 48827-48833.

Wang, T. C., Cardiff, R. D., Zukerberg, L., Lees, E., Arnold, A., and Schmidt, E. V. (1994). Mammary hyperplasia and carcinoma in MMTV-cyclin D1 transgenic mice. Nature *369*, 669-671.

(11) APPENDICES

Venkataramani, R.N., MacLachlan, T.K, Chai, X., El-Deiry, W.S. and Marmorstein, R. "Structure-Based Design of More Stable $p18^{INK4c}$ Proteins with Increased CDK Inhibitory Activity." (2002), *J. Biol. Chem.*, 277, 48827-48833.

THE JOURNAL OF BIOLOGICAL CHEMISTRY
Vol. 277, No. 50, Issue of December 13, pp. 48827–48833, 2002

Printed in U.S.A.

Structure-based Design of p18^{INK4c} Proteins with Increased Thermodynamic Stability and Cell Cycle Inhibitory Activity*

Received for publication, August 7, 2002, and in revised form, October 3, 2002
Published, JBC Papers in Press, October 4, 2002, DOI 10.1074/jbc.M208061200

Ravichandran N. Venkataramani‡§, Timothy K. MacLachlan¶, Xiaomei Chai‡, Wafik S. El-Deiry¶, and Ronen Marmorstein‡§‖**

From the ‡The Wistar Institute, the ¶Howard Hughes Medical Institute, the §Department of Biochemistry and Molecular Biophysics, and the ‖Department of Chemistry, University of Pennsylvania, Philadelphia, Pennsylvania 19104

p18^{INK4c} is a member of the INK4 family of proteins that regulate the G_1 to S cell cycle transition by binding to and inhibiting the pRb kinase activity of cyclin-dependent kinases 4 and 6. The p16^{INK4a} member of the INK4 protein family is altered in a variety of cancers and structure-function studies of the INK4 proteins reveal that the vast majority of missense tumor-derived p16^{INK4a} mutations reduce protein thermodynamic stability. Based on this observation, we used p18^{INK4c} as a model to test the proposal that INK4 proteins with increased stability might have enhanced cell cycle inhibitory activity. Structure-based mutagenesis was used to prepare p18^{INK4c} mutant proteins with a predicted increase in stability. Using this approach, we report the generation of three mutant p18^{INK4C} proteins, F71N, F82Q, and F92N, with increased stability toward thermal denaturation of which the F71N mutant also showed an increased stability to chemical denaturation. The x-ray crystal structures of the F71N, F82Q, and F92N p18INK4C mutant proteins were determined to reveal the structural basis for their increased stability properties. Significantly, the F71N mutant also showed enhanced CDK6 interaction and cell cycle inhibitory activity *in vivo*, as measured using co-immunoprecipitation and transient transfection assays, respectively. These studies show that a structure-based approach to increase the thermodynamic stability of INK4 proteins can be exploited to prepare more biologically active molecules with potential applications for the development of molecules to treat p16^{INK4a}-mediated cancers.

Progression through the cell cycle is monitored at the G_1-S phase checkpoint by active complexes between cyclin-dependent kinases (CDK)[1] 4 and 6 and the D-type cyclins (D1, D2, D3). The INK4 family of proteins plays a key role in inhibiting the G_1-S phase cell cycle transition by specifically inhibiting the kinase activity of CDK4-Cyclin D and CDK6-Cyclin D complexes. The INK4 (inhibitors of CDK4) family of proteins consists of four known members: p16^{INK4a}, p15^{INK4b}, p18^{INK4c}, and p19^{INK4d}, which share 40% sequence identity overall and structural homology (1–5).

The INK4 family members have indistinguishable CDK/cyclin inhibitory activity when assayed *in vitro* (6), but appear to have distinct functions *in vivo*. For example, the locus on 9p21 (MTS1) expressing p16^{INK4a} is a frequent target of genetic alterations in cancer, while the genes encoding the other INK4 proteins are much less commonly mutated in cancer. Specifically, gene deletions in MTS1 and promoter methylation often lead to transcriptional silencing, and point mutations are frequently associated with several different types of cancer (7–10). Nearly 55 different residues are targeted in missense mutations of p16^{INK4a} (7). Homozygous deletions of p15^{INK4b} have also been identified in a more limited number of cancer cell lines (11), and point mutations of p18^{INK4c} have been associated with some breast carcinomas (12). Homozygous deletions of the p18^{INK4c} are also observed in oligodendrogliomas (13); however, these deletions are rare. Polymorphisms of the p19^{INK4d} gene are found in a small percentage of osteosarcomas (14). Together, the data on tumor-derived mutations suggest tissue-specific, and/or non-redundant activities for the INK4 proteins (15).

Significant insights into the mechanism of INK4-mediated inhibition of cyclin-CDK complexes and the deleterious effects of tumor-derived mutations on their kinase inhibitory properties come from structural analyses of the INK4 proteins. The INK4 proteins contain four or five ankyrin repeat motifs that contain a β-strand helix-turn-helix β-strand segment that associates with neighboring motifs through β-sheet and helical bundle interactions. The ankyrin repeats stack on top of each other to form an elongated overall structure in which the helical region is along one side of the protein and the β-sheet region is along the opposite side (16, 17). A mapping of p16^{INK4a} tumor-derived mutations onto the INK4 protein structures reveal that most of these mutations localize to residues involved in ankyrin repeat conformation or interrepeat interactions (17), suggesting that a large percentage of p16^{INK4a} mutations decrease the stability of the protein. Indeed, several of these mutations lead to the decreased stability of p16^{INK4a} and p18^{INK4c} proteins when studied *in vitro* (18–21). Together, these studies suggest that the decreased thermostability of p16^{INK4a} correlate with its loss of function and tumorigenic properties.

The structure of INK4 proteins in binary complex with CDK6 (22, 23) and in ternary complex with CDK6 and a D-type viral cyclin (24) reveal that the INK4 protein binds next to the ATP

* This work was supported by Grant RPG-98-235-GMC from the American Cancer Society, Grant DAMD17-02-1-0725 from the U. S. Army Department of Defense Breast Cancer Program (to R. M.), and Research Fellowship Grant DAMD17-98-1-8270 from the U. S. Army Department of Defense Breast Cancer Program (to R. N. V.). The costs of publication of this article were defrayed in part by the payment of page charges. This article must therefore be hereby marked "*advertisement*" in accordance with 18 U.S.C. Section 1734 solely to indicate this fact.

The atomic coordinates (code 1MX2, 1MX4, and 1MX6) have been deposited in the Protein Data Bank, Research Collaboratory for Structural Bioinformatics, Rutgers University, New Brunswick, NJ (http://www.rcsb.org/)

** To whom correspondence should be addressed. Tel.: 215-898-5006; Fax: 215-898-0381; E-mail: marmor@wista.wistar.upenn.edu.

[1] The abbreviations used are: CDK, cyclin-dependent kinase; INK4, inhibitors of CDK4.

binding site of the CDK. The resulting distortion of the kinase catalytic cleft prevents ATP binding and thereby inhibits catalysis (25). While, each of the first 4 ankyrin-repeat units of the INK4 proteins participate in CDK4 interaction, most of the interactions are mediated by the 2nd and 3rd ankyrin repeat units. In addition, comparison of the INK4 structures in the presence or absence of CDK reveals that the INK4 protein does not undergo significant structural rearrangement for CDK binding with an overall RMS deviation of less than 1.3 Å.

Based on the structure-function studies described above for the INK4 proteins, we hypothesized that we may be able to use a structure-based approach to prepare mutant INK4 proteins with increased stability and increased CDK4/6 and cell cycle inhibitory activity. The preparation of INK4 proteins with increased CDK4 inhibitory properties would potentially be useful for targeting p16^{INK4a}-mediated cancers and would provide a proof-of-principle for the design of "biophysical drugs" (small molecule compounds that may reactivate tumor derived p16^{INK4a} mutants by modifying the biophysical properties of the protein such as stability). Indeed, the design of such compounds for the reactivation of tumor-derived mutants of the p53 tumor suppressor has already been described (26).

As both the native and complexed structures of p18^{INK4c} have been described (17, 24), we used p18^{INK4c} as the INK4 model of choice to carry out the initial structure-function studies. Since the INK4 proteins are highly homologous, we expect that the results of our studies with p18^{INK4c} would be transferable to other INK4 proteins such as p16^{INK4a}. In this report we describe the preparation, and functional and structural characterization of single-site mutant p18^{INK4c} proteins that are designed for increased stability. Through this study, we have identified at least one mutant, the F71N p18^{INK4c} mutant that has significantly increased stability *in vitro* and enhanced CDK4/6 and cell cycle inhibitory activity *in vivo*. We discuss the implications of these findings for improving the thermodynamic stability of the INK4 proteins as a means to increase their cell cycle inhibitory activities, and for the development of compounds for the treatment of p16^{INK4a}-mediated cancers.

MATERIALS AND METHODS

Cloning and Protein Purification—Single amino acid substitutions in p18^{INK4c} were produced using the QuickChange mutagenesis kit (Stratagene) using the pRSETA-p18^{INK4c} vector (17) as a template, and sequence changes were confirmed by DNA sequencing. Recombinant native and mutant p18^{INK4c} proteins were prepared by growing and inducing pRSETA-p18^{INK4c} (native or mutant) transformed BL21 (DE3) cells at 37 °C. Cells were lysed and purified in a low salt buffer (LSB) containing 50 mM Tris (pH 8.5), 50 mM NaCl, 5 mM β-mercaptoethanol, and 0.1 mg ml^{-1} phenylmethylsulfonyl fluoride. Except for the F71N p18^{INK4c} mutant, all other recombinant proteins (including the native protein) were isolated by renaturing the protein found in the inclusion bodies with 6 M urea denaturation and renaturation by stepwise dialysis to remove urea. The soluble fraction from renaturation was further purified by cation exchange with a Q-Sepharose fast flow column (Amersham Biosciences) and gel filtration using a Superdex-75 column (Amersham Biosciences) (17). The F71N p18^{INK4c} mutant was the only protein that was found exclusively in the soluble protein fraction, and the supernatant was directly purified using cation exchange and gel filtration chromatography (17). Protein aliquots were flash-frozen at −70 °C and thawed as needed for biophysical studies or crystallization.

Circular Dichroism-monitored Thermal Denaturation—Circular dichroism data for the thermal denaturation studies was collected on an AVIV circular dichroism spectrophotometer (Model 62A-DS) equipped with a thermoelectric unit and using a 1-mm pathlength cell. Thermal protein denaturation was monitored at 222 nm and was shown to be irreversible. Data was collected every 2 °C with an equilibrium time of 4 min and an averaging time of 10 s. Protein samples were analyzed at a concentration of 2 mg ml^{-1} (~20 μM) in 50 mM HEPES pH 7.5. Protein concentrations were determined using UV spectrophotometry. However, concentration of the W5R mutant, which had a low extinction coefficient, was determined using a Bradford assay using the native protein as a standard. The melting temperature, T_m and error estimates were calculated by fitting the denaturation data (molar ellipticities) to a non-linear dose-response logistical transition $\{y = a_0 + a_1/(1 + x/a_2)^{a3})\}$ using the Levenberg-Marquardt algorithm within the SlideWrite software package, where the a_2 coefficient is T_m.

Circular Dichroism-monitored Urea Denaturation—Circular dichroism data for the urea denaturation studies was collected on a Jasco J-720 spectopolarimeter at 25 °C. The CD signal at 222 nm was recorded using a 100-μl cell containing a 0.2-mm pathlength. Protein samples were at a concentration of 2 mg/ml in a buffer containing 20 mM HEPES, 100 mM NaCl, and urea concentrations from 0–6 M in increments of 0.5 M. Samples were equilibrated for 4 h (equilibration was shown to be complete after 3 h, data not shown) prior to analysis by CD, and all samples were prepared and recorded in duplicate yielding an average CD value that was used for all subsequent analysis. The fraction of unfolded protein (f_u) as a function of urea concentration was calculated with the equation $f_u = ([\theta_{222}]_{obs} - [\theta_{222}]_f)/([\theta_{222}]_u - [\theta_{222}]_f)$, where $[\theta_{222}]_{obs}$ is the molar helical ellipticity at a particular urea concentration and $[\theta_{222}]_f$ and $[\theta_{222}]_u$ are the helical ellipticities of the fully folded protein (in the absence of denaturant) and the fully unfolded protein (in the presence of high urea concentrations), respectively. $[\theta_{222}]_f$ and $[\theta_{222}]_u$ were determined at the base lines of the transition curves at which $[\theta_{222}]_{obs}$ became relatively invariant at changing urea concentrations. The free energy of unfolding, ΔG_D, for each of the partially unfolded states were calculated assuming a two sate unfolding transition using the equation $\Delta G_D = -RT\ \ln(K_u)$, where $K_u = ([\theta_{222}]_{obs} - [\theta_{222}]_f)/([\theta_{222}]_u - [\theta_{222}])$, and ΔG_D (H_20) and m (change in free energy of unfolding with urea concentration) was calculated by fitting the data to a straight line with the equation $\Delta G_D = \Delta G_D(H_20) + m[\text{urea}]$ (27).

Crystallization and Structure Determination of p18^{INK4c} Mutants—Crystallization of the F71N, F82Q, and F92N p18^{INK4c} mutants were carried out by vapor diffusion at room temperature, using 2-μl hanging drops containing 5 mg ml^{-1} protein, 20 mM Tris (pH 8.5), 0.5 mM dithiothreitol, 7% PEG 6000 (polyethylene glycol, average molecular mass 6000 M_r), and 1 M NaCl equilibrated over a reservoir containing 14% PEG 6000 and 2 M NaCl. These conditions are similar to those used to crystallize the native protein. Crystals grew to a typical size of 100–200 μm × 75–150 μm × 50–100 μm in the space group $P2_12_12$, with cell dimensions that are isomorphous with the native p18^{INK4c} crystals (a = 55.6 Å, b = 151.6 Å, c = 40.5 Å and $\alpha = \beta = \gamma = 90°$). Crystals were transferred to a harvest solution (HS) containing 20 mM Tris (pH 8.5), 15% PEG 6000 and 2 M NaCl, transferred stepwise to HS supplemented with 25% glycerol, and frozen in liquid nitrogen-cooled liquid propane prior to data collection.

Diffraction data was collected at 110 K using a Rigaku Raxis IV image plate detector with CuKα radiation from a Rigaku RU-300 generator, and the data was processed and scaled using DENZO and SCALEPACK (28). The structural coordinates of native p18^{INK4c} were used as a starting model for the mutant proteins. The position and orientation of these coordinates was initially adjusted using rigid body refinement with the program CNS (29). Model building was carried out using the program O (30) using omit maps and sigma A weighted 2 $F_o - F_c$ and $F_o - F_c$ difference Fourier maps created with the program CNS (29). Iterative rounds of model building followed by positional refinement, simulated annealing (31), and torsion angle dynamic (32) refinement protocols were carried out at successively higher resolution shells. At the final resolution shell, solvent molecules were added, and the final model was checked for errors with simulated annealing omit maps, omitting 10 residues at a time (33). The resulting protein structures have excellent refinement statistics and geometry (Table IV).

In Vivo p18^{INK4c} Stability and CDK6 Association—DNA encoding wild-type and mutant p18^{INK4c} proteins were subcloned into the pCDNA3.1 vector creating a set of pCDNA- p18^{INK4c} vectors (T85F was not tested due to complications in the subcloning). The cell culture conditions of the U2OS cells were essentially as described (34). A total of 1×10^6 U2OS cells were transfected using Superfect reagent (Qiagen Inc., Valencia, CA) with 0.5 μg of green fluorescent protein reporter and 1.5 μg of pCDNA-p18^{INK4c} (native or mutant), pCDNA-p21, or vector alone. After 24 h post-transfection, the cells were lysed, and the proteins were separated on a 15% SDS-PAGE. The proteins were blotted onto nitrocellulose filter paper and probed with anti-p18^{INK4c} antiserum (Oncogene Research), followed by horseradish-conjugated anti-rabbit IgG antibody. The reacting p18^{INK4c} bands were detected using enhanced chemiluminescence reagent for direct comparison of the *in vivo* stability of wild-type and mutant p18^{INK4c} proteins.

The relative amount of wild-type and mutant p18^{INK4c} protein that is associated with CDK4/6 *in vivo* was determined using CDK6 co-immu-

TABLE I
Properties of p18^{INK4c} residues targeted for mutagenesis

Residue	Rationale for mutation	Mutation	Predicted change in thermostability	Interaction with residues in CDK6[a]	Conservation among INK4 proteins
Trp-5	Exposed hydrophobic	Arg	Increase	No	No
Phe-37	Exposed hydrophobic	His	Increase	Yes, non-polar side chain contacts	Yes
Arg-55	Buried hydrophilic	Val	Increase	No	No
Phe-71	Exposed hydrophobic, possible inter-repeat contacts	Asn	Increase	Yes, non-polar side chain contacts	No
His-75	Buried polar	Phe	Decrease	No	Yes
Phe-82	Exposed hydrophobic, possible inter-repeat contacts	Gln	Increase	Yes, non-polar side chain contacts	Yes
Thr-85	Buried polar	Phe	Decrease	No	Yes
Phe-92	Exposed hydrophobic, possible inter-repeat contacts	Asn	Increase	No	No
His-108	Buried polar	Leu	Decrease	No	Yes

[a] Based on p18^{INK4c} interactions with CDK6 as reported in the ternary complex with viral cyclin (24).

noprecipitation experiments. The p18^{INK4c}-transfected U2OS cells were lysed and endogenous CDK6 was immunoprecipitated with CDK6 antiserum (BD PharMingen). These immunoprecipitates were analyzed on 15% SDS-PAGE, and the gels were blotted and probed with anti-p18^{INK4c} antiserum, followed by horseradish-conjugated anti-rabbit IgG antibody. The cell lysis was carried out in the presence of two different salt concentrations (150 mM and 250 mM) prior to immunoprecipitation to optimize the discrimination between the differing binding affinities of the p18^{INK4c} mutants for CDK6.

In Vivo Cell Cycle Inhibition Assay—For cell cycle analysis, p18^{INK4c}-transfected cells were prepared in 1% fetal bovine serum/phosphate-buffered saline for fluorescence-activated cell sorting (FACS) analysis after 24 h. Preparation of cells for fluorescence-activated cell sorting was performed essentially as described (35). Cell sorting was performed on a Coulter Epics Elite counter. DNA content analysis was performed using MacCycle software (Phoenix Flow Systems, San Diego, CA).

RESULTS AND DISCUSSION

Design of p18^{INK4c} Mutant Proteins—The high-resolution crystal structure of p18^{INK4c}, was used to identify candidate residues for mutation. The strategy for the mutagenesis was to increase the hydrophobicity of the protein interior or to increase the hydrophilicity of the protein exterior. Accordingly, buried hydrophilic residues were changed to hydrophobic residues or exposed hydrophobic residues were changed to hydrophilic residues. In mutating hydrophobic residues to hydrophilic residues, mutations were selected to facilitate interactions with residues in neighboring repeats. Moreover, buried hydrophilic residues were mutated to hydrophobic residues of similar size that were predicted to facilitate favorable interactions with other hydrophobic residues in its vicinity. With the aid of the program O (36), we modeled several mutations choosing the ones that best fit the criteria described above. The nine mutations that were made, along with their corresponding degree of conservation and structural properties, are listed in Table I and illustrated on a schematic of the overall p18^{INK4c} structure in Fig. 1. 5 of the 9 mutations selected are conserved among the INK4 proteins (Phe-37, His-75, Phe-82, Thr-85, and His-108). Six of the mutations were designed to increase the thermodynamic stability of p18^{INK4c}, and a subset of these residues are also predicted to be at the INK4-CDK interface based on the INK4 co-crystal structures (Phe-37 (F37H), Phe-71 (F71N), and Phe-82 (F82Q)) (22–24). Therefore, while one set of mutations are predicted to have effects only on the thermodynamic stability of p18^{INK4c}, another subset are predicted to have effects on both the thermodynamic stability of p18^{INK4c} and interaction with CDK. As negative controls, 3 of 9 mutations were also prepared that were predicted to decrease the thermodynamic stability of p18^{INK4c}, these include His-75 (H75F), His-108 (H108L), and Thr-85 (T85F).

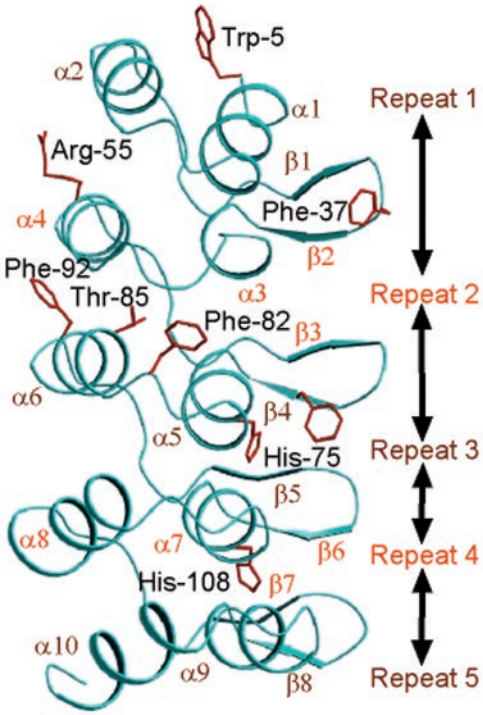

FIG. 1. **Residues of p18^{INK4c} targeted for mutations.** The ankyrin repeat elements are shown in alternating *red* and *orange*, and the residues targeted for mutations are shown in red.

Characterization of the p18^{INK4c} Mutant Protein during Purification and Crystallization—When expressed in bacteria, some mutants behave significantly differently than the native protein. These mutants include F71N, F82Q, and F92N. Bacterial growths prepared at 37 °C revealed that these mutants are found in the soluble fraction of the bacterial lysate whereas the native protein is found exclusively in the insoluble fraction when the bacteria are grown at 37 °C. Surprisingly, F71N is found exclusively in the soluble fraction, while about 25% of F82Q and F92N are found in the soluble fraction (Table II). Each of the proteins were purified essentially as described for the native protein and eluted from gel filtration in monomeric form. Following protein purification, all three of these proteins crystallize at room temperature (at 20 °C), while the native protein precipitates when crystal trials are carried out at the same temperature. Despite the different crystal growth temperature, crystals of the three mutant proteins are isomorphous with crystals of the native protein that are obtained from the same crystallization condition, but at 4 °C (Table II and

TABLE II
Biochemical characterization of p18^{INK4c} mutants

Construct	Solubility of protein from bacterial lysates[a]	Ability to renature protein[b]	Oligomerization state[c]	Crystallization[d]
Native	Insoluble	Yes	Monomer	Yes at 4 °C
W5R	Insoluble	Yes	Monomer	N.D.[e]
F37H	Insoluble	Yes	Monomer	N.D.
R55V	Insoluble	Yes	Monomer	N.D.
F71N	100% soluble	NT[f]	Monomer	Yes at 20 °C
H75F	Insoluble	Yes	Aggregated	N.D.
F82Q	~25% soluble	Yes	Monomer	Yes at 20 °C
T85F	Insoluble	Yes	Mixture of aggregates and monomer	N.D.
F92N	~25% soluble	Yes	Monomer	Yes at 20 °C
H108L	Insoluble	Yes	Mixture of aggregates and monomer	N.D.

[a] The solubility of the protein refers to the presence of the protein in either the soluble or insoluble fractions of the bacterial lysate when the protein is overexpressed at 37 °C.
[b] The ability to renature the protein refers to whether the protein can be isolated in the soluble fraction after denaturation by 6 M urea followed by stepwise dialysis to remove urea.
[c] Molecular size is judged by size exclusion chromatography of the renatured protein.
[d] Crystallization was only carried out with a few mutants; the crystals so obtained were isomorphous to the crystals of the native protein.
[e] Not determined.
[f] Not tested.

Table III). The increased solubility properties of the F71N, F82Q, and F92N mutant proteins suggested that they might also be more thermostable than the native protein.

Native p18^{INK4c} and each of the other mutant proteins were found exclusively in the insoluble protein fraction from a bacterial preparation that was grown at 37 °C. Upon renaturation and subsequent purification, most of these proteins eluted as monomers from gel filtration chromatography. However, the T85F and H108L mutants yielded mixtures of aggregates and monomeric protein, while the H75F mutant protein yielded aggregated protein exclusively. Taken together, these results suggested that the three mutants, H75F, T85F, and H108L might be thermodynamically less stable than the native protein.

Thermodynamic Stability of p18^{INK4c} Protein Mutants in Vitro—CD-monitored thermal denaturation was used to qualitatively characterize and compare the thermodynamic stabilities of p18^{INK4c} and its mutant proteins. Since the p18^{INK4c} protein has substantial helical content, the CD signal at a wavelength of 222 nm, which is sensitive to helix formation, could be monitored as a function of solution temperature to develop a melting isotherm for each protein. The melting profiles for the native and mutant p18^{INK4c} proteins are compared in Fig. 2*a*, and the respective melting temperatures that are derived from these profiles are tabulated in Table III. These data reveal that of the 8 mutant p18^{INK4c} proteins that could be purified to homogeneity, 3 were clearly more stable to thermal denaturation than the native protein while 3 were clearly less thermostable; while two proteins, F37H and R55V, exhibited comparable thermostability as the native protein. The p18^{INK4c} mutants that were most stable to thermal denaturation included F71N, F92N, and F82Q; and the melting temperature of these mutants are ~4 °C higher than the native protein (p value < 0.001). The less stable class of mutants contains three mutants, W5R, T85F, and H108L with melting temperatures from 4 to 17 °C less than the native protein (p value < 0.001). The H75F mutant may belong in the less stable category of p18^{INK4c} mutants; however, it was too unstable to be purified for further characterization (Table II and Table III).

TABLE III
Thermodynamic parameters of p18^{INK4c} and mutants

Protein	T_m[a]	U_m[b]	ΔG_U^{H2O}[c]	m
	°C	M	kcal mol^{-1}	kcal mol^{-1} M^{-1}
F71N	45.96 ± 0.03	2.98 ± 0.07	3.41	1.17
F92N	45.81 ± 0.22	2.36 ± 0.04	1.62	0.71
F82Q	45.31 ± 0.14	2.43 ± 0.02	2.24	0.90
F37H	42.28 ± 0.11	2.66 ± 0.05	1.46	0.72
R55V	42.15 ± 0.01	2.76 ± 0.02	2.38	0.84
Native p18^{INK4c}	41.53 ± 0.56	2.74 ± 0.05	2.70	1.00
W5R	37.86 ± 0.05	N.D.	N.D.	N.D.[d]
T85F	33.93 ± 0.08	N.D.	N.D.	N.D.
H108L	24.55 ± 0.23	N.D.	N.D.	N.D.
H75F				

[a] Midpoint of thermal unfolding transition.
[b] Midpoint of urea unfolding transition.
[c] Free energy of unfolding at 23 °C (296 K) with estimated error as calculated from the urea unfolding data and extrapolated to zero urea concentration.
[d] Not determined.

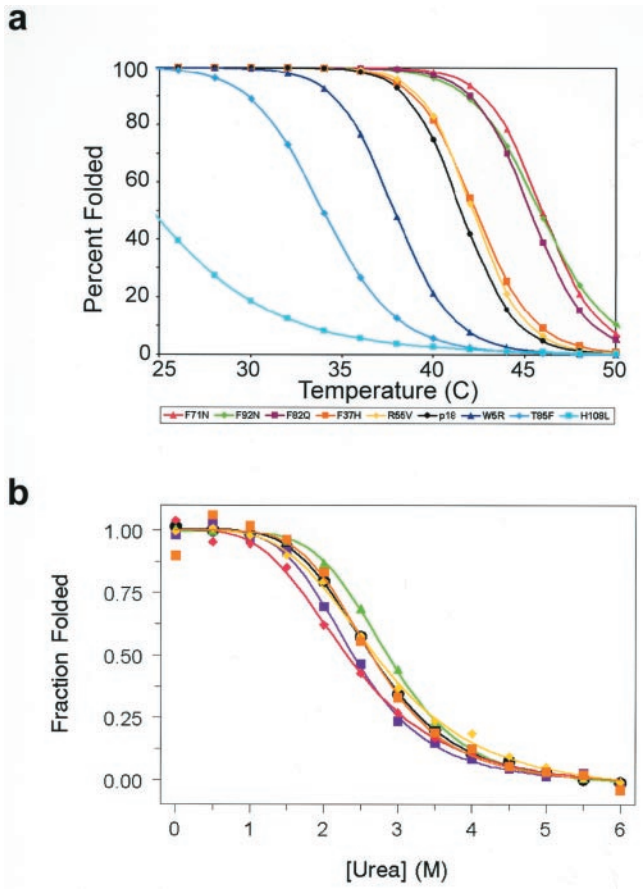

FIG. 2. **Denaturation profiles of native and mutant p18^{INK4c} proteins.** *a*, thermal denaturation of native and mutant p18^{INK4c} proteins. The mean at each temperature of duplicate experiments are shown here. The S.D. of the data was very small due to the reproducibility of the data; therefore, error bars are not shown. The mutants are color-coded *below* the figure. *b*, urea-induced denaturation of native and mutant p18^{INK4c} proteins. The mean at each urea concentration of duplicate experiments are shown here. The color-coding of mutants is the same as in *a*.

To more quantitatively assess the thermodynamic stability of p18^{INK4c} and the mutants that showed increased thermal stability, these proteins were analyzed with CD spectroscopy using chemical denaturation with urea. The urea-induced unfolding profiles for the native and mutant p18^{INK4c} proteins are compared in Fig. 2*b*, and the respective urea concentrations required to unfold 50% of the respective protein are tabulated

TABLE IV
Summary of crystallographic data and refinement parameters

	F71N	F82Q	F92N
Data statistics			
Resolution range	50.0–2.25	50.0–2.0	50–2.0
Unique reflections	22,638	22,818	22,869
R_{sym} (%)	8.5	3.9	6.2
I/σ	15.19	23.87	10.10
Completeness (%)	92.7	97.7	96.6
Refinement statistics			
Protein atoms	2376	2404	2376
Water atoms	192	179	174
R factors			
R_{free}	25.4	26.0	26.3
$R_{working}$	21.4	23.1	23.7
Model statistics			
Root mean square values			
Bond length	0.004	0.005	0.006
Bond angles	1.19	1.24	1.34
NCS molecules	0.819	0.756	0.745
Average *B* factors	19.51	25.69	26.61

in Table III. In addition, the urea unfolding data was used to calculate the free energy of unfolding [$\Delta G(H_2O)$] and m (Table III). Correlating with the thermal denaturation studies, the most thermostable p18^{INK4c} mutant, F71N, was also the most stable to chemical denaturation. Specifically, this mutant was about 0.71 kcal/mol more stable than the native protein. Interestingly, the other p18^{INK4c} mutants that showed increased stability toward thermal denaturation did not exhibit increased stability toward chemical denaturation (Table III). A correlation of these results with the aggregation properties of the recombinant p18^{INK4c} mutants prepared and purified from bacteria (Table II) suggests that the increased thermal stability of the F82Q and F92N p18^{INK4c} mutants might be due to their lower propensities to aggregate relative to the native protein. This would be consistent with their higher T_m (which would be affected by protein aggregation) without a corresponding increase in stability due to urea denaturation (which should be independent of protein aggregation).

Structural Characterization of the p18^{INK4c} Mutant Proteins, F71N, F82Q, and F92N—To determine the structural basis for the enhanced stability properties of the three p18^{INK4c} mutants; F71N, F82Q, and F92N, we determined their high resolution crystal structures.

F71N—The structure of the F71N p18^{INK4c} mutant was determined to a resolution of 2.25 Å (Table IV). Position 71 in p18^{INK4c} is located in the β4 strand and at the beginning of ankyrin repeat 3. The structure shows that asparagine 71 directly hydrogen bonds with arginine 79 in the α5 helix in the middle of the ankyrin repeat and also makes a water-mediated hydrogen bond with Asp-100 in the β5 strand at the end of the ankyrin repeat (Fig. 3, *a* and *b*). Taken together, the F71N p18^{INK4c} mutation allows new intra-ankyrin repeat interactions that stabilize the tight turns in the structure resulting in the increased stability of the mutant protein.

The structure of the p18^{INK4c}/CDK-cyclin complex reveals that although phenylalanine 71 does not interact with CDK, it is nonetheless at the binding interface. Therefore, it is possible that an asparagine substitution at this position would also introduce favorable p18^{INK4c}-CDK contacts. Modeling studies suggests that an asparagine at position 71 would be in position to interact with a backbone NH of CDK (glycine 36 of CDK6). Interestingly, other INK4 proteins have a threonine in the corresponding position, which also does not participate in CDK interaction in the p16^{INK4a} and p19^{INK4d} complexes with CDK (22, 23). Taken together, it is therefore likely that an asparagine substitution in other INK4 proteins would increase their thermodynamic stabilities and possibly also their CDK interaction and cell cycle inhibitory activities.

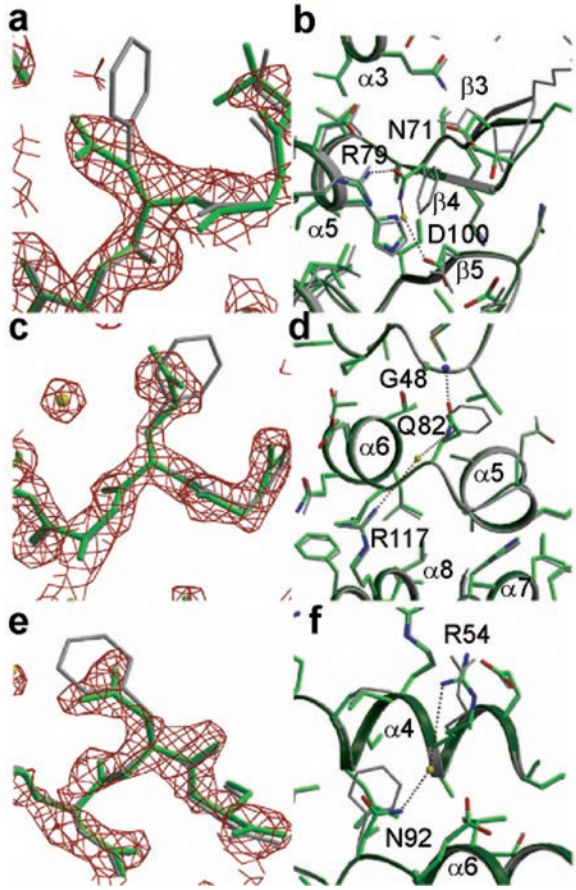

FIG. 3. **Structure of the F71N, F82Q, and F92N p18^{INK4c} mutants in comparison to the native structure of p18^{INK4c} protein.** *a*, superposition of the mutant, F71N (in *green*) and the native protein (in *gray*) along with the simulated annealing omit map around the site of mutation contoured at 1.5σ. The *yellow sphere* represents a water molecule. *b*, detailed interactions made in the F71N p18^{INK4c} mutant are shown in *green* with CPK coloring, while the structure of the native protein, which lacks these new interactions are shown in *gray*. The mutation results in a new hydrogen-bonding interaction with arginine 79, and a water (shown in *yellow*)-mediated hydrogen bond with aspartate 100. Glycines are shown as *green* or *gray* spheres. *c*, same as *a* except that the F82Q mutant is shown. *d*, detailed interactions made in the F82Q p18^{INK4c} mutant are shown in green with CPK coloring, while the structure of the native protein, which lacks these, new interactions are shown in *gray*. The mutation results in new hydrogen bonding interaction with the backbone NH of glycine 48 and a water (shown in *yellow*)-mediated hydrogen bond with arginine 117. Glycines are shown as *green* or *gray* spheres. *e*, same as *a* except that the F92N mutant is shown. *f*, detailed interactions made in the F92N p18^{INK4c} mutant are shown in *green* with CPK coloring, while the structure of the native protein, which lacks these, new interactions are shown in *gray*. The mutation results in a new water-mediated hydrogen bond with arginine 54. Glycines are shown as *green* or *gray* spheres. Molscript objects for the electron density was created using CONSCRIPT, and the figures were prepared with the programs MOLSCRIPT (37) and RASTER3D (38).

F82Q—The crystal structure of the F82Q mutant was determined to 2.0 Å resolution (Table IV). In the native protein, phenyalanine 82 is located in the turn between the α5 and α6 helices of ankyrin repeat 3. The structure of the glutamine mutant reveals that the glutamine at position 82 hydrogen bonds to the backbone nitrogen of glycine 48 on the turn between the α3 and α4 helices of ankyrin repeat 2. The glutamine mutant also makes a water-mediated hydrogen bond to arginine 117 in helix α8 in ankyrin repeat 4 (Fig. 3, *c* and *d*).

Therefore, the glutamine mutation in position 82 of p18^{INK4c} appears to increase the thermal stability of the p18^{INK4c} protein by increasing inter-ankyrin repeat interaction.

The structure of the INK4/CDK complexes reveals that phenylalanine 82 makes a van der Waals contact with the CDK. Indeed, the fact that this residue is strictly conserved within the INK4 family supports its functional importance. Possibly, the aliphatic region of the glutamine may mimic the van der Waals interaction that is mediated by the native phenyalanine residue. In addition, modeling studies suggests that glutamine 82 is in position to make a backbone NH hydrogen bond with the CDK (Ser-155 of CDK6).

F92N—The structure of the F92N mutant was determined to 2.0 Å resolution (Table IV). Position 92 is located on the loop following the α6 helix of the third ankyrin repeat. Glutamine 92 participates in a water-mediated hydrogen bond with arginine 54 that is located on the α4 helix on the second ankyrin repeat (Fig. 3, *e* and *f*). In addition, this new interaction might stabilize the turn from α-helix 6 to the adjacent loop. Therefore, the mutation F92N appears to facilitate new inter-ankyrin repeat interactions that stabilize a tight turn in the structure resulting in the increased thermal stability of the mutant. Interestingly, unlike the F71N and F82Q p18^{INK4c} mutants that were in position to mediate interactions with CDK, the F92N mutation is unlikely to effect interaction with CDK since it is located too far from the binding interface.

In Vivo Characterization of p18^{INK4c} Protein Mutants—To determine if the increased *in vitro* stability of the p18^{INK4c} mutants is correlated with increased stability and CDK6 binding activity *in vivo*, we transfected plasmids encoding each of the mutants into U2OS cells for functionally characterization. Twenty four hours post-transfection, the *in vivo* stability of the wild-type and mutant p18^{INK4c} proteins was assayed using Western blots to p18^{INK4c} and the relative association of these proteins with CDK6 was assayed using co-immunoprecipitation with CDK6, followed by Western analysis for p18^{INK4c} (Fig. 4*a*). As predicted, this analysis shows that the three-p18INK4c mutants that are most thermostable *in vitro* (F71N, F82Q, and F92N) are also more stable and more tightly associated to CDK6 *in vivo*. Moreover, one of the least stable p18^{INK4c} mutants, H108L, had significantly decreased *in vivo* stability and CDK6 association.

Interestingly, one of the p18^{INK4c} mutants that we were unable to purify in recombinant form due to protein instability, H75F, was relatively stable *in vivo* and also associated relatively strongly with CDK6. It is possible that this mutant, although unstable in nascent form, may form an unusually stable complex with CDK6, which would explain its increased *in vivo* stability. Moreover, the structure of the CDK6/INK4 complexes (22–24) shows that although the position that corresponds to histidine 75 of p18^{INK4c} does not directly participate in CDK interaction, it is in position to do so if minor side chain rearrangements of either the INK4 of CDK proteins were to take place. Therefore, it is possible that a histidine to phenylalanine substitution in p18^{INK4c} would introduce a new (and particularly stable) interaction between p18^{INK4c} and the CDK. Further analysis will be required to understand the behavior of the H75F p18^{INK4c} mutant. Nevertheless, the results of the *in vivo* experiments described above generally correlate with the relative thermostability of the p18^{INK4c} mutants when assayed *in vitro*.

To directly determine whether the more stable p18^{INK4c} mutants were indeed more potent cell cycle inhibitors, we subjected the wild-type and mutant p18^{INK4c}-transfected cells to FACS analysis. As expected from the stability studies, each of

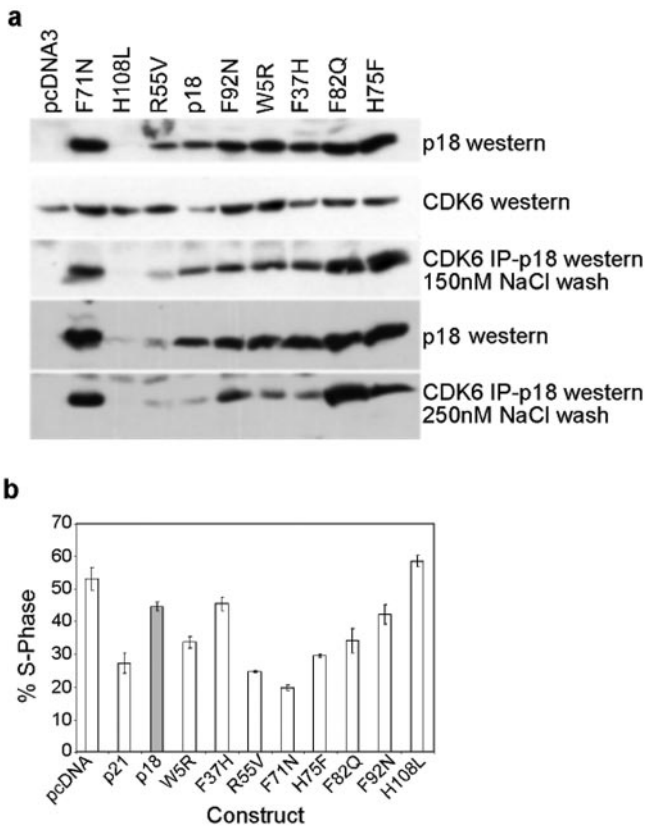

FIG. 4. **In vivo activity of p18^{INK4c} and mutants.** *a*, U2OS cells that are transiently transfected with either wild-type or mutant p18^{INK4c} are assayed for relative p18^{INK4c} levels using Western analysis with anti-p18^{INK4c} antiserum. These cells are also used to compare the relative amount of p18^{INK4c} and mutants that are associated with CDK4/6 *in vivo* using co-immunoprecipitation experiments with anti-CDK6 followed by a buffer washing and analysis with anti-p18^{INK4c} antiserum. Two experiments are shown, one with buffer washing containing 150 mM NaCl and another at a more stringent buffer washing of 250 mM NaCl. *b*, comparison of p18^{INK4c} with the mutants showing the percent of U2OS cells in S-phase after 24 h of transient transfections (along with 95% confidence intervals). The vector pcDNA and CDK inhibitor, p21 are shown as negative and positive controls respectively. The native p18^{INK4c} is shaded in *gray* while the mutants are arranged in the order of their position in the p18^{INK4c} protein sequence. The transfection experiments were performed four times, and in each experiment native or mutant expression vectors was transfected in triplicate flasks. For each cell cycle analysis from each individual transfection, 10,000–20,000 GFP-positive cells were analyzed. The data presented represents the aggregate analysis using all experiments performed, including the confidence intervals (calculated from S.D. estimates) of the mean.

three most thermostable p18^{INK4c} mutants (F71N, F82Q, and F92N) were also more potent cell cycle inhibitors when assayed *in vivo* (Fig. 4*b*). The F71N mutant, that showed the greatest thermal and chemical stability (both *in vitro* and *in vivo*), also showed the most potent cell cycle inhibitory activity, showing a direct correlation between stability and cell cycle inhibitory activity by this p18^{INK4c} mutant.

Interestingly, the thermostability and cell cycle inhibitory activity of some of the other p18^{INK4c} mutants did not strictly correlate. For example, both the F37H and R55V p18^{INK4c} mutants showed thermodynamic properties similar to the native protein (Fig. 2 and Table III). However, the *in vivo* cell cycle inhibition assay shows that while the F37H p18^{INK4c} mutant is a slightly weaker cell cycle inhibitor than the native protein, the R55V mutant is a significantly more potent cell cycle inhibitor (Fig. 4*b*). Results such as these are not that surprising since several factors that can play a role in the *in vivo* cell cycle activity of the p18^{INK4c} mutant proteins are not

accounted for, including their relative affinities for CDK6 and any indirect effects that these mutants may have on cell cycle inhibition. Nonetheless, these results show that the stability of p18^{INK4c} can be exploited to create more potent cell cycle inhibitory proteins, and that a structure-based approach can be used to facilitate this process.

Implications for Rescuing Tumor-derived INK4 Mutations—We have used a structure-based approach to successfully prepare p18^{INK4c} proteins containing single site mutations that are more stable *in vitro*, and that are more potent cell cycle inhibitors *in vivo* than the native protein. Of the single-site p18^{INK4c} mutant proteins that we prepared, of particular interest is the F71N mutation. This protein was thermodynamically more stable to thermal and chemical denaturation *in vitro* and the most potent cell cycle inhibitor *in vivo*. Since an asparagine substitution was chosen arbitrarily (within the constraints of a charged residue) there is a possibility that mutation to another residue may create an even more thermodynamically stable and potent p18^{INK4c} cell cycle inhibitor. For example, the F71N structure shows that the asparagine residue from ankyrin repeat 3 forms a direct hydrogen bound with arginine 79 within the same ankyrin repeat and makes an additional water-mediated hydrogen bond with aspartic acid 100 at the beginning of the 4th ankyrin repeat (Fig. 3, *a* and *b*). This latter interaction may be more important for protein stability since it increases the interaction between neighboring ankyrin repeats. In light of this, a glutamine substitution may work better than an asparagine substitution toward increasing the proteins thermostability. Modeling of a glutamine suggests that it would still be able to mediate the arginine 79 interactions and in addition would be long enough to make a direct interaction with aspartic acid 100, rather than the water-mediated interaction that is made with the asparagine substitution. Using a similar structure based strategy; we would predict that a glutamine substitution at position 92 would also increase the thermal stability of p18^{INK4c} even more than the asparagine mutation introduced in the F92N mutant. In addition, although we do not yet have structures for the p18^{INK4c} mutants R55V and F37H, the relatively modest increase in thermal stability of these mutants relative to the wild type protein suggests that other mutations may have more pronounced enhancements in protein stability. Taken together, the studies presented here provide an excellent starting point for the use of site-directed mutagenesis, including combining favorable mutations, for the design of more thermostable and active p18^{INK4c} proteins that can be further refined with additional structure-based mutagenesis.

We would expect that at least some of the results obtained in this study can be extended to the homologous p16^{INK4a} protein, and that introduction of similar mutations into p16^{INK4a} would result in a more potent cell cycle inhibitor and tumor suppressor. Such "enhanced" p16^{INK4a} proteins may be ideal candidates for a gene therapy approach to help treat p16^{INK4a} -mediated cancers. Moreover, the studies presented here provide a proof of principle that small molecule compounds may be prepared that can mimic the effect of some of the mutations described here and may function to reactivate tumor-derived p16^{INK4a} mutations.

Acknowledgments—We thank Yelena Shifman for technical assistance and David Speicher and Kehao Zhao for useful discussions.

REFERENCES

1. Guan, K.-L., Jenkins, C. W., Li, Y., Nichols, M. A., Wu, X., O'Keefe, C. L., Matera, A. G., and Xiong, Y. (1994) *Genes Dev.* **8,** 2939–2952
2. Chan, F. K. M., Zhang, J., Cheng, L., Shapiro, D. N., and Winoto, A. (1995) *Mol. Cell. Biol.* **15,** 2682–2688
3. Hannon, G. J., and Beach, D. (1994) *Nature* **371,** 257–261
4. Kamb, A., Gruis, N. A., Weaver-Feldhaus, J., Liu, Q., Harshman, K., Tavtigian, S. V., Stockert, E., III, R. S. D., Johnson, B. E., and Skolnick, M. H. (1994) *Science* **264,** 436–440
5. Serrano, M., Hannon, G. J., and Beach, D. (1993) *Nature* **366,** 704–707
6. Hirai, H., Roussel, M. F., Kato, J. Y., Ashmun, R. A., and Sherr, C. J. (1995) *Mol. Cell. Biol.* **15,** 2672–2681
7. Smith-Sorensen, B., and Hovig, E. (1996) *Human Mutat.* **7,** 294–303
8. Kamb, A., Shattuck-Eidens, D., Eeles, R., Liu, Q., Gruis, N. A., Ding, W., Hussey, C., Tran, T., Miki, Y., Weaver-Feldhaus, J., McClure, M., Aitken, J. F., Anderson, D. E., Bergman, W., Frants, R., Goldgar, D. E., Green, A., Maclennan, R., Martin, N. G., Meyer, L. J., Youl, P., Zone, J. J., Skolnick, M. H., and Cannon-Albright, L. A. (1994) *Nat. Genet.* **8,** 22–26
9. Pollock, P. M., Pearson, J. V., and Hayward, N. K. (1996) *Genes Chromosom. Cancer* **15,** 77–88
10. Okuda, T., Shurtleff, S. A., Valentine, M. B., Raimondi, S. C., Head, D. R., Behm, F., Curcio-Brint, A. M., Liu, Q., Pui, C. H., and Sherr, C. J. (1995) *Blood* **85,** 2321–2330
11. Gemma, A., Takenoshita, S., Hagiwara, K., Okamoto, A., Spillare, E. A., Mcmemamin, M. G., Hussain, S. P., Forrester, K., Zariwala, M., Xiong, Y., and Harris, C. C. (1996) *Int. J. Cancer* **68,** 605–611
12. Lapointe, J., Lachance, Y., Labrie, Y., and Labrie, C. (1996) *Cancer Research* **56,** 4586–4589
13. Pohl, U., Cairncross, J. G., and Louis, D. N. (1999) *Brain Pathology* **9,** 639–643
14. Miller, C. W., Yeon, C., Aslo, A., Mendoza, S., Aytac, U., and Koeffler, H. P. (1997) *Oncogene* **15,** 231–235
15. Roussel, M. F. (1999) *Oncogene* **18,** 5311–5317
16. Luh, F. Y., Archer, S. J., Domaille, P. J., Smith, B. O., Owen, D., Brotherton, D. H., Raine, A. R. C., Xu, X., Brizuela, L., Brenner, S. L., and Laue, E. D. (1997) *Nature* **389,** 999–1003
17. Venkataramani, R., Swaminathan, K., and Marmorstein, R. (1998) *Nat. Struct. Biol.* **5,** 74–81
18. Yang, R., Gombart, A. F., Serrano, M., and Koeffler, H. P. (1995) *Cancer Res.* **55,** 2503–2506
19. Ruas, M., Brookes, S., McDonald, N. Q., and Peters, G. (1999) *Oncogene* **18,** 5423–5434
20. Tevelev, A., Byeon, I.-J. L., Selby, T., Ericson, K., Kim, H.-J., Kraynov, V., and Tsai, M.-D. (1996) *Biochemistry* **35,** 9475–9487
21. Zhang, B., and Peng, Z.-y. (1996) *J. Biol. Chem.* **271,** 28734–28737
22. Russo, A. A., Tong, L., Lee, J.-O., Jeffrey, P. D., and Pavletich, N. P. (1998) *Nature* **395,** 237–243
23. Brotherton, D., Dhanaraj, V., Wick, S., Brizuela, L., Domaille, P. J., Volyanik, E., Xu, X., Parisini, E., Smith, B. O., Archer, S. J., Serrano, M., Brennen, S. L., Blundell, T. L., and Laue, E. D. (1998) *Nature* **395,** 244–250
24. Jeffrey, P. D., Tong, L., and Pavletich, N. P. (2000) *Genes Dev.* **14,** 3115–3125
25. Pavletich, N. P. (1999) *J. Mol. Biol.* **287,** 821–828
26. Foster, B. A., Coffey, H. A., Morin, M. J., and Rastinejad, F. (1999) *Science* **286,** 2507–2510
27. Pace. (1986) *Methods Enzymol.* **131,** 266–280
28. Gewirth, D., Otwinowski, Z., and Minor, W. (1993) *The HKL Version 1.0 manual* (3rd, Ed.), Yale University Press, New Haven, CT
29. Brunger, A. T., Adams, P. D., Clore, G. M., DeLano, W. L., Gros, P., Grosse-Kunstleve, R. W., Jiang, J. S., Kuszewski, J., Nilges, M., Pannu, N. S., Read, R. J., Rice, L. M., Simonson, T., and Warren, G. L. (1998) *Acta Crystallogr.* **D54,** 905–921
30. Jones, T. A., Zou, J. Y., and Cowen, S. W. (1991) *Acta Crystallogr.* **A47,** 110–119
31. Brunger, A. T., and Krukowski, A. (1990) *Acta Crystallogr.* **A46,** 585–593
32. Rice, L. M., and Brunger, A. T. (1994) *Proteins* **19,** 277–290
33. Brunger, A. T., Kuriyan, J., and Karplus, M. (1987) *Science* **235,** 458–460
34. Somasundaram, K., Zhang, H., Zeng, Y. X., Houvras, Y., Peng, Y., Wu, G. S., Licht, J. D., Weber, B. L., and El-Deiry, W. S. (1997) *Nature* **389,** 187–190
35. van den Heuvel, S., and Harlow, E. (1993) *Science* **262,** 2050–2054
36. Jones, T. A., and Kjeldguard, M. (1996) *Manual for O, Version 6.1*, Aarhus University Press, Uppsula, Sweden.
37. Kraulis, P. J. (1991) *J. Appl. Cryst.* **24,** 946–950
38. Merritt, E. A., and Murphy, M. E. P. (1994) *Acta Cryst.* **D50,** 869–873